Probing CO_2 reaction mechanisms and effects on the $SrNb_{0.1}Co_{0.9-x}Fe_xO_{3-\delta}$ cathodes for solid oxide fuel cells

Yinlong Zhu [a], Jaka Sunarso [b], Wei Zhou [a,*], Zongping Shao [c,*]

[a] State Key Laboratory of Materials-Oriented Chemical Engineering, College of Chemistry & Chemical Engineering, Nanjing Tech University, No. 5 Xin Mofan Road, Nanjing 210009, People's Republic of China
[b] Department of Chemistry, University of Waterloo, 200 University Avenue West, Waterloo, Ontario N2L 3G1, Canada
[c] State Key Laboratory of Materials-Oriented Chemical Engineering, College of Energy, Nanjing Tech University, No. 5 Xin Mofan Road, Nanjing 210009, People's Republic of China

ARTICLE INFO

ABSTRACT

Solid oxide fuel cell (SOFC) can convert chemical to electrical energy with high efficiency and low emission. In addition to the efforts to lower the operating temperature of SOFC to below 650 °C, the availability of CO_2 resistant-cathode materials is envisioned to increase the practicality of the device for dual-chamber SOFC application using ambient air and also for single-chamber SOFC application using hydrocarbons. In this work, we evaluate CO_2 resistance of $SrNb_{0.1}Co_{0.9-x}Fe_xO_{3-\delta}$ ($x = 0$, 0.1, 0.2, 0.3, 0.5 and 0.9) and the reaction mechanisms using complementary characterization techniques, e.g., powder X-ray diffraction (XRD), Fourier transform-infra red (FT-IR) spectroscopy and CO_2-temperature programmed desorption (CO_2-TPD). Increasing amount of Fe on the perovskite lattice resulted in the increased resistance (less sensitivity) to CO_2 as reflected by less change in area specific resistance (ASR) values after CO_2 exposure. The trend can be rationalized by the increase in the average metal-oxygen bond energy (ABE) imparted by the stronger Fe—O bond (relative to Co—O bond). Powder XRD could not detect the presence of carbonate phase on all compositions after 1 h of CO_2 exposure at 600 °C. After pro-longed exposure, up to 60 h, $SrCO_3$ was found on SNCF0.1 while remained absent on SNC. FT-IR spectra showed the evidence of carbonate vibrations only for SNCF0.1, SNCF0.2 and SNCF0.3. The appearance of an extra peak for these compositions on their CO_2-TPD profiles is likely related to the carbonate decomposition which was not observed on SNC, SNCF0.5 and SNF profiles. These complementary data led us to conclude two different mechanisms i.e., CO_2 adsorption accompanied by formation of strontium carbonate occurred on SNCF0.1, SNCF0.2 and SNCF0.3 whereas only CO_2 adsorption occurred on SNC, SNCF0.5 and SNF. The higher oxygen non-stoichiometry for the former three compositions (with respect to the latter three compositions) correlates with the tendency to form carbonate, suggesting that oxygen vacancies can promote the formation of carbonates.

© 2015 Elsevier B.V. All rights reserved.

1. Introduction

Carbondioxide (CO_2) effects on the cathode of solid oxide fuel cell (SOFC) are often overlooked despite its importance toward the device practical value. Current research direction of conventional dual-chamber SOFC (DC-SOFC, e.g., cathode is exposed to oxidant and anode is exposed to fuel) is largely focused on lowering its operating temperature. By decreasing the temperature to below 650 °C, the cost of the device is reduced while intercon-

nects and sealing materials' options are widened in addition to attaining increased maximum theoretical efficiency, rapid start-up and thermal cycling capability and lower performance degradation [1]. Since at these temperatures, oxygen reduction in cathode side is the limiting factor, the relevant undertakings have manifested in the development of various high-performance cathode materials such as $Ba_{0.5}Sr_{0.5}Co_{0.8}Fe_{0.2}O_{3-\delta}$ (BSCF), $SrNb_{0.1}Co_{0.9}O_{3-\delta}$ (SNC), $SrSc_{0.2}Co_{0.8}O_{3-\delta}$ (SSC), $Sr_{0.95}Nb_{0.1}Co_{0.9}O_{3-\delta}$ (SNC0.95), $SrSc_{0.175}Nb_{0.025}Co_{0.8}O_{3-\delta}$ (SSNC) [2–6]. Most of these perovskite materials however contain alkaline earth metals which form carbonates upon contact with CO_2. Such carbonate formation, in turn, negatively affects their oxygen exchange kinetics and simultaneously deteriorates their original structure [7–9]. Take BSCF in CO_2-containing atmosphere for example, significant

* Corresponding authors. Tel.: +86 25 83172256; fax: +86 25 83172242.
E-mail addresses: sailseeker@163.com (W. Zhou), shaozp@njtech.edu.cn (Z. Shao).

carbonate formation happens between 300 and 800 °C, particularly at 300–400 °C, surface passivation occurs followed by substantial CO_2 uptake at 600–800 °C [9]. While regeneration (e.g., thermal carbonate decomposition and CO_2 desorption from the perovskite lattice) is possible and is enhanced in CO_2-free atmosphere, this process is kinetically favored only above 800 °C. Within this context, which is more or less identical for other alkaline-earth based perovskites, given that ambient air also contains CO_2 (although at very low concentration), the practical values of BSCF and these alkaline-earth based perovskite materials below 650 °C become questionable [9–12].

Single-chamber SOFC (SC-SOFC) represents another attractive SOFC concept requiring CO_2-resistant cathode materials [13,14]. Because SC-SOFC operates with only one gas chamber, both the anode and cathode are exposed to the mixture of fuel and oxidant gases and the resultant reaction products such as CO_2; the concentration of which can reach 10% by volume [15]. This device is more attractive than dual-chamber one in terms of a more compact cell stack and less complicated manifold configuration as well as self-sustaining temperature (from the fuel reaction with oxidant). Methane can be used directly as a fuel without carbon deposition problem (e.g., coking) and the use of higher hydrocarbons (e.g., ethane, propane and butane) in fact improves the cell performance below 500 °C. SC-SOFC can also be coupled with Gd-Ni catalysts to co-generate electricity and synthesis gas (CO and H_2) and recover energy from engine exhaust [16,17].

Clear correlation between the extent of CO_2 effect to the structure and performance of perovskite oxide and the metal components of the perovskite has yet to be fully established. Thermodynamically, Ellingham diagram (and the respective CO_2 chemical potential) can be used to evaluate the stability of carbonates for different metals (such as Ba, Sr, Ca and La) at a certain CO_2 partial pressure and temperature [8,18]. This diagram suggests that $BaCO_3$ is more readily formed than $SrCO_3$ and $CaCO_3$. Accordingly, Ba-based perovskites is more susceptible to CO_2 [19–21]. Another important perspective for the reaction between perovskite and CO_2 is based on Lewis acid-base theory where CO_2 and metal oxide acts as the acid and base, respectively. Making use of this theory, the intensity of the reaction can be determined by the basicity (e.g., the ability to donate electrons to CO_2) of the metal oxide which varies at different temperature and pressure [7,22]. Although the basicity of the metal oxide can be measured using binding energy of oxygen (e.g., O1s) from X-ray Photoelectron Spectroscopy (XPS) data, metal bond strength (or energy) serves as a more simple quantification parameter due to its close relation with the basicity. Higher basicity is generally reflected by the lower bond strength. For example, Ta—O, Fe—O and Co—O bond strength was reported as 384.5, 390.4 and 799.1 kJ mol^{-1}, respectively; consistent with the increased CO_2 stability from $SrCoO_{3-\delta}$ to $Sr(Co,Fe)O_{3-\delta}$ and then to $Sr(Co,Fe,Ta)O_{3-\delta}$ [7].

We have recently reported a novel perovskite family, $SrNb_{0.1}Co_{0.9-x}Fe_xO_{3-\delta}$ for cathode of low temperature SOFC [23]. These cathodes are of interest not only for their high oxygen reduction reaction activity at 600 °C and below but also for their CO_2 resistance. This work provides a more systematic study on the effect of CO_2 on $SrNb_{0.1}Co_{0.9-x}Fe_xO_{3-\delta}$ cathodes (x = 0, 0.1, 0.2, 0.3, 0.5 and 0.9; denoted as SNC, SNCF0.1, SNCF0.2, SNCF0.3, SNCF0.5 and SNF, respectively). Based on the characterization results, two different mechanisms are proposed to explain the interaction between CO_2 and the perovskites in CO_2-containing atmosphere. For SNC, SNCF0.5 and SNF, CO_2 adsorption occurs with negligible formation of $SrCO_3$ whereas for SNCF0.1, SNCF0.2 and SNCF0.3, both CO_2 adsorption and $SrCO_3$ formation took place. Identical trend for the mechanisms and the oxygen non-stoichiometry (e.g., the non-stoichiometry for SNC, SNCF0.5 and SNF is substantially lower relative to SNCF0.1, SNCF0.2 and SNCF0.3) implies dominant role of

oxygen vacancies toward facilitating reaction with CO_2. Moreover, we also showed that the average metal-oxygen bond energy can be utilized as a good predictor for CO_2 resistance trend.

2. Experimental

2.1. Synthesis of powder

$SrNb_{0.1}Co_{0.9-x}Fe_xO_{3-\delta}$ (x = 0, 0.1, 0.2, 0.3, 0.5 and 0.9) powders were synthesized by solid-state reaction route. Stoichiometric amounts of $SrCO_3$, Nb_2O_5, Co_2O_3 and Fe_2O_3 (all of analytical grade, Sinopharm Chemical Reagent Co., Ltd.) were weighed and thoroughly mixed in a ball mill (Fritsch, Pulverisette 6) in acetone medium at 400 rpm for 1 h. After drying, the milled powders were calcined at 1200 °C in air for 10 h. The milling and calcination were conducted twice to obtain highly pure $SrNb_{0.1}Co_{0.9-x}Fe_xO_{3-\delta}$ powders for characterization.

2.2. Fabrication of the symmetrical cell

Symmetrical cells with electrode $Sm_{0.2}Ce_{0.8}O_{1.9}$ (SDC) electrode configuration were fabricated for electrochemical impedance spectroscopy (EIS) measurements. Dense SDC disks of 12 mm in diameter and 0.8 mm thickness were prepared by dry pressing 0.5 g of powder followed by sintering at 1400 °C for 5 h. The cathode powders were first dispersed in a pre-mixed solution of glycerol, ethylene glycol and isopropyl alcohol. A colloidal suspension was made from these mixtures by planetary milling (Fritsch, Pulverisette 6) at 400 rpm for 0.5 h. The suspension was deposited by spray deposition onto both sides of the SDC disk and calcined at 1000 °C for 2 h in air atmosphere to obtain porous electrodes. As current collector, silver paste was painted onto the electrode and dried at 100 °C.

2.3. Characterisation

Crystal structures of the powder were determined by powder X-ray diffraction (Bruker D8 Advance, Germany) with filtered Cu-Kα radiation at 40 kV and 40 mA using a receiving slit of approximately 0.2–0.4 mm. Powder X-ray diffraction patterns were collected by step scanning at 2θ = 10 − 90° with a step size of 0.05°. The oxygen non-stoichiometry of the powders at room temperature was quantified using iodometric titration. In brief, about 0.1 g of powder was dissolved in a 6 mol L^{-1} HCl solution in nitrogen atmosphere to prevent the oxidation of I$^-$ ions (from KI) by air followed by titration using a standard thiosulfate ($S_2O_3{}^{2-}$) solution. For the Fourier transform-infra red (FT-IR) spectroscopy, powders were mixed with KBr and pressed into disks. The FT-IR analyses were performed on a NEXUS-670 FT-IR spectrometer (Thermo Nicolet, USA) in the frequency range of 400–4000 cm^{-1} with a resolution of 2 cm^{-1} and a scanning number of 150. The spectra were collected using the KBr contained disks in transmission mode. CO_2 desorption properties of the powders were evaluated using CO_2 temperature programmed desorption (CO_2-TPD). In a typical CO_2-TPD experiment, about 0.15 g of powder (previously screened through 40–60 meshes sieves to remove large powder particles) was loaded into a U-type quartz tube. Pure argon at a flow rate of 15 ml min^{-1} (STP) was fed into the reactor as the carrier gas while the temperature was increased from room temperature to 930 °C using a ramp rate of 10 °C min^{-1}. The effluent gases were analysed in terms of their CO_2 concentration using a mass spectrometer (MS, Hiden, QIC-20).

2.4. Electrochemical measurement

The electrochemical impedance spectra (EIS) of the symmetrical cells were acquired using Solartron 1287 and 1260 A electrochem-

ical workstations. The applied frequency range was from 0.01 Hz to 100 kHz, and the signal amplitude was 10 mV under open cell voltage conditions. The symmetrical cells were tested 600 °C in air prior and after introducing different concentration of CO_2 (e.g., 1, 5 and 10% by volume) into the air atmosphere.

2.5. Calculation of the average metal-oxygen bond energy

The average metal (A, B)-oxygen bond energy (<ABE>) within the perovskite lattice was obtained from the average A—O (<A—O>) and B—O (<B—O>) bond energy. The <A—O>, <B—O> and <ABE> for $A_{1-x}A'_xB_{1-y-z}B'_yB_zO_{3-\delta}$ compounds were calculated as follows [24]:

(the following equations for A', B' and B can be applied similarly to A and B)

$$< ABE > = < A\text{—}O > + < B\text{—}O > \qquad (1)$$

$$< A\text{—}O > = \Delta(A\text{—}O) + \Delta(A'\text{—}O) \qquad (2)$$

$$< B\text{—}O > = \Delta(B\text{—}O) + \Delta(B'\text{—}O) + \Delta(B''\text{—}O) \qquad (3)$$

$$\Delta(A\text{—}O) = x_A/(CN_A \times m) \times (\Delta H_{AmOn} - m \times \Delta H_A - n/2 \times D_{O2}) \qquad (4)$$

$$\Delta(B\text{—}O) = x_B/(CN_B \times m) \times (\Delta H_{BmOn} - m \times \Delta H_B - n/2 \times D_{O2}) \qquad (5)$$

In these equations, x_A and x_B represents molar fraction of A and B metal, respectively; $\Delta H_{A(B)mOn}$ and $\Delta H_{A(B)}$ represents the enthalpy of formation of one mole of A(B)mOn and the sublimation energy of A(B) metal at 25 °C obtained from the thermodynamic data, respectively [25]. For $SrNb_{0.1}Co_{0.9-x}Fe_xO_{3-\delta}$, $\Delta H_{Sr} = 163.856$ kJ mol^{-1}, $\Delta H_{Nb} = 721.05$ kJ mol^{-1}, $\Delta H_{Co} = 428.032$ kJ mol^{-1}, $\Delta H_{Fe} = 415.74$ kJ mol^{-1}; $\Delta H_{SrO} = -591.47$ kJ mol^{-1}, $\Delta H_{Nb2O5} = -1897.72$ kJ mol^{-1}, $\Delta H_{Co2O3} = -653.1$ kJ mol^{-1}, $\Delta H_{Fe2O3} = -820.534$ kJ mol^{-1}; $CN_{A(B)}$ represents the coordination number of cations at A and B site ($CN_A = 12$, $CN_B = 6$); D_{O2} represents the dissociation energy of O_2 (e.g., 500.2 kJ mol^{-1}).

3. Results and discussion

The oxygen reduction reaction (ORR) activity is reflected by the area specific resistance (ASR) value. In this case, ASR was measured using impedance spectroscopy of the symmetrical cell of $SrNb_{0.1}Co_{0.9-x}Fe_xO_{3-\delta}$ |$Sm_{0.2}Ce_{0.8}O_{1.9}$ (SDC)| $SrNb_{0.1}Co_{0.9-x}Fe_xO_{3-\delta}$ with x varying from 0 to 0.9. Sensitivity of ASR to CO_2, in turn, was tested by monitoring the ASR value of the cathode at 600 °C in air prior and after introducing different concentration of CO_2 (e.g., 1, 5 and 10% by volume) into the air atmosphere as depicted in Fig. 1a. We find that for most compositions, the ASR increased quite rapidly at first 3–5 min and then kept increasing but much slower. As a general trend, higher CO_2 concentration induces higher ASR values (lower ORR activity). We hypothesize that CO_2 is not only adsorbed onto the perovskite surface but also reacts with the metal component of the perovskite to form carbonate, which resulted in the reduction of the active sites for ORR [26–29]. In addition, we notice that Co substitution by Fe provides better CO_2 resistance. The relative increases of ASR values for each composition after ~1 h (57 min) exposure to CO_2 containing atmosphere (with the procedure described in Fig. 1a) compared to the original values in air are displayed in Fig. 1b. These values vary between 2 and 4 for Fe-containing compositions as opposed to ~15 for Co-based composition. This trend is consistent with the higher bond energy for Fe—O relative to Co—O or equivalently, lower basicity for Fe-containing compositions relative to Co-based one [7,30].

To probe the reaction between CO_2 and the perovskites, $SrNb_{0.1}Co_{0.9-x}Fe_xO_{3-\delta}$ ($0 \leq x \leq 0.9$) powders were exposed to pure CO_2 at 600 °C for 1 h. These powders were then analyzed using powder X-ray diffraction (XRD) and Fourier-transform infrared
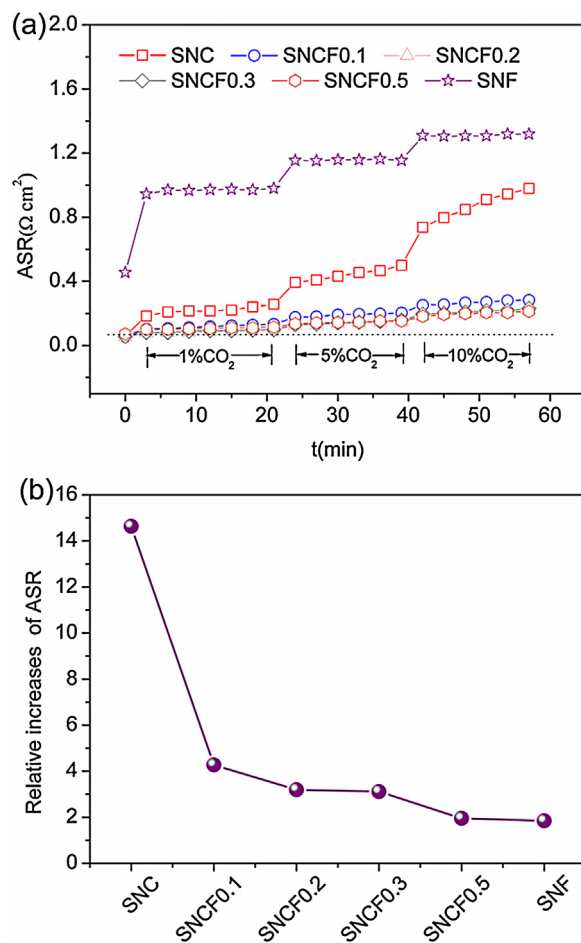

Fig. 1. (a) Time-dependent area specific resistance of $SrNb_{0.1}Co_{0.9-x}Fe_xO_{3-\delta}$ electrodes as a function of CO_2 concentration in air at 600 °C. (b) Relative increases of area specific resistances of $SrNb_{0.1}Co_{0.9-x}Fe_xO_{3-\delta}$ after ~1 h exposure to CO_2 containing atmosphere compared to the original values in air.

spectroscopy (FT-IR). Fig. 2a shows the powder XRD patterns which indicate that the original cubic structures were retained. These patterns however provide no indication of carbonate phase (e.g., no characteristic peaks of carbonate phase). Perhaps, the concentration of the carbonate phase is too low to be detected by XRD. When the exposure period was further increased up to 60 h, a low intensity peak characteristic of $SrCO_3$ appeared on SNCF0.1 pattern (Fig. 2b). This indicates that during the additional hours, substantial amount of $SrCO_3$ was formed on SNCF0.1. For SNC, the absence of such peak rules out the carbonate formation in large amount. The latter observation on SNC nonetheless was cross-checked using FT-IR spectroscopy, a sensitive technique to detect the presence of CO_3^{2-} [31]. Fig. 2c and d show the FT-IR spectra of $SrNb_{0.1}Co_{0.9-x}Fe_xO_{3-\delta}$ powders before and after CO_2 exposure for 1 h at 600 °C. As a baseline, the FT-IR spectrum of $SrCO_3$ was obtained and shown in Supporting Information (Fig. s1). It is notable that all $SrNb_{0.1}Co_{0.9-x}Fe_xO_{3-\delta}$ powders were subjected to identical conditions during FT-IR spectroscopy to ensure valid semi-quantitative comparison. Characteristic vibration bands of carbonate group (most likely from $SrCO_3$) at 1440 cm^{-1} and 860 cm^{-1} were evident for SNCF0.1, SNCF0.2 and SNCF0.3 (Fig. 2d) [10,27]. Upon comparing the band intensity, the amount of $SrCO_3$ phase is likely to decrease in the order of SNCF0.1, SNCF0.2 and SNCF0.3. These vibration bands, on the other hand, are absent on the FT-IR spectra for SNC, SNCF0.5 and SNF (Fig. 2d). Hence, the FT-IR results attest to the exclusive carbonate formation on SNC,
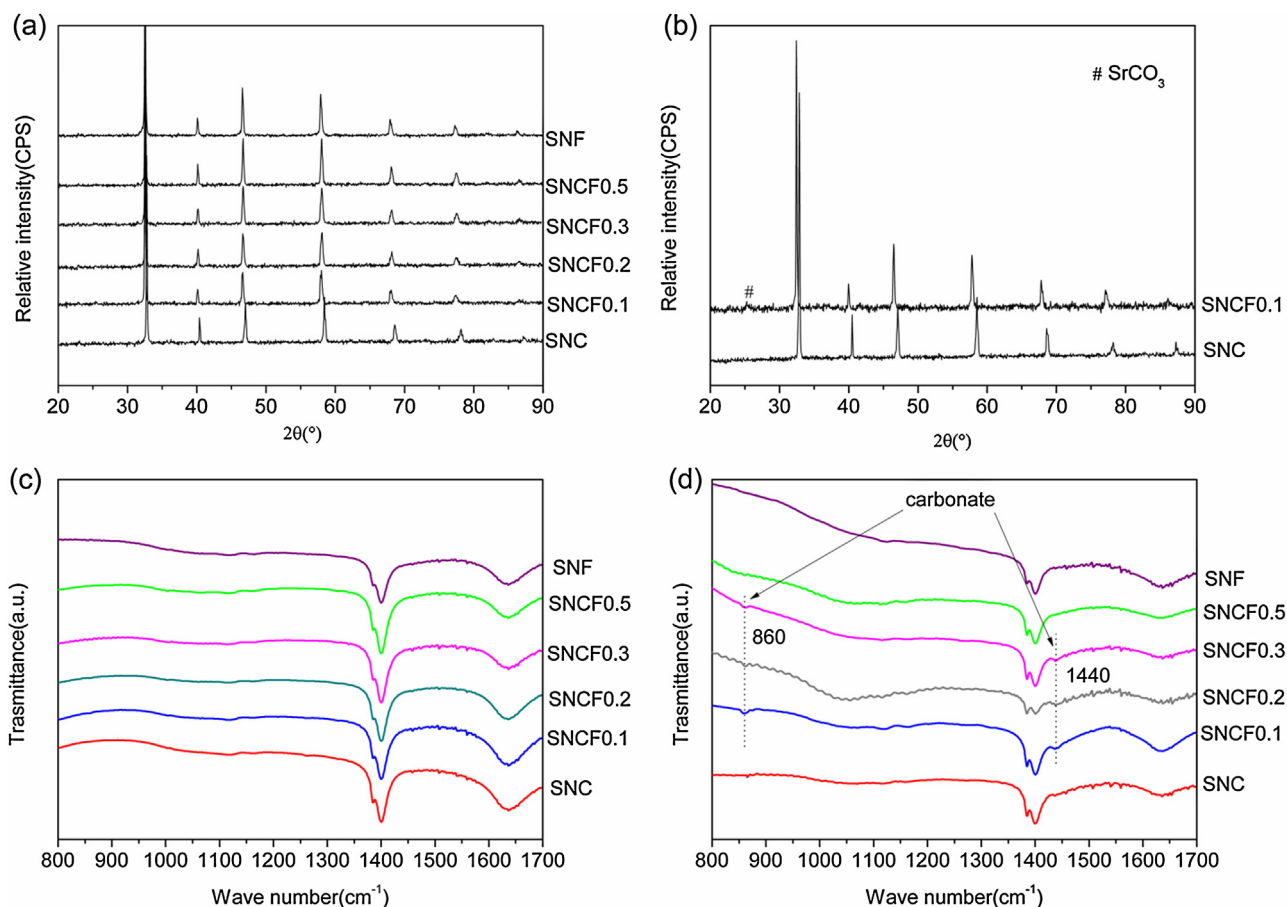
Fig. 2. Powder X-ray diffraction patterns of (a) $SrNb_{0.1}Co_{0.9-x}Fe_xO_{3-\delta}$ powders after exposure to ultra high purity CO_2 (99.999%) for 1 h at 600 °C; and (b) SNC and SNCF0.1 powders after exposure to ultra high purity CO_2 for 60 h at 600 °C; Fourier transform-infra red spectra of $SrNb_{0.1}Co_{0.9-x}Fe_xO_{3-\delta}$ powders (c) before and (d) after exposure to ultra high purity CO_2 for 1 h at 600 °C.

SNCF0.5 and SNF during 1 h of exposure to ultra high purity CO_2 (99.999%) at 600 °C.

The interaction between the perovskite surface and adsorbed molecules was further evaluated using temperature programmed desorption (TPD) equipped with mass spectrometer [20,29,31]. Fig. 3 depicts the CO_2-TPD profiles of $SrNb_{0.1}Co_{0.9-x}Fe_xO_{3-\delta}$
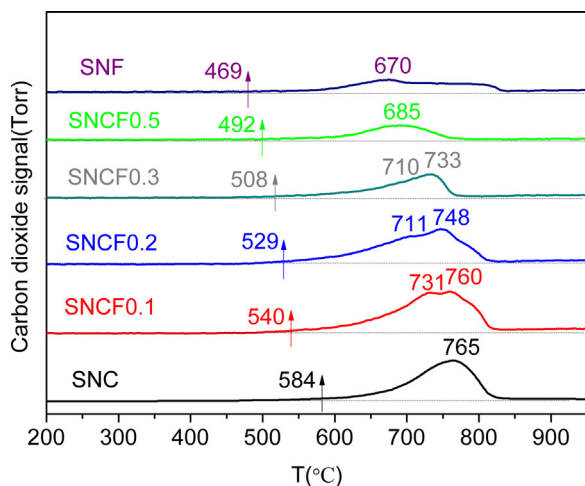

Fig. 3. CO_2-temperature programmed desorption profiles of $SrNb_{0.1}Co_{0.9-x}Fe_xO_{3-\delta}$ powders after exposure to ultra high purity CO_2 for 1 h at 600 °C.

($0 \leq x \leq 0.9$) powders after exposure to ultra high purity CO_2 for 1 h at 600 °C. The CO_2-TPD profile of $SrCO_3$ was also collected (Fig. s2) which indicates the onset decomposition temperature of 720 °C. Two overlapped desorption peaks appear on the profiles of SNCF0.1, SNCF0.2 and SNCF0.3, unlike the profiles of SNC, SNCF0.5 and SNF which display one major peak. Although the 1st peak is less apparent on SNCF0.3 profile, the left long-tail of the skewed curve suggests that a different process to the 2nd one occurred over this section. The two peaks essentially correspond to the decomposition of $SrCO_3$ and the release of adsorbed CO_2; the trend of which is additionally consistent with the FT-IR results. The onset temperature is, in fact, decreases with increasing Fe content, as does the peak temperature and the area. It becomes apparent that Fe, due to its stronger bonding with O, facilitates the CO_2 desorption, or equivalently, suppresses CO_2 adsorption into the surface of the perovskite [7,30].

Excellent agreement between the results from powder XRD, FT-IR and CO_2-TPD leads to the conception of two different mechanisms for interaction of CO_2 and $SrNb_{0.1}Co_{0.9-x}Fe_xO_{3-\delta}$ perovskites in CO_2-containing atmospheres, shown schematically in Fig. 4. Whereas CO_2 adsorption and carbonate formation occurred on the surface of SNC0.1, SNCF0.2 and SNCF0.3, there is only CO_2 adsorption took place on the surface of SNC, SNCF0.5 and SNF. The most plausible reason for the distinct mechanism we can think of is the oxygen vacancies. Previous reports claimed substantial role of oxygen vacancies toward the carbonate formation on the surface of perovskites, e.g., BSCF, $LaFeO_{3-\delta}$ and $(Ba,Ca)(Co,Fe)O_{3-\delta}$ [20,32,33].
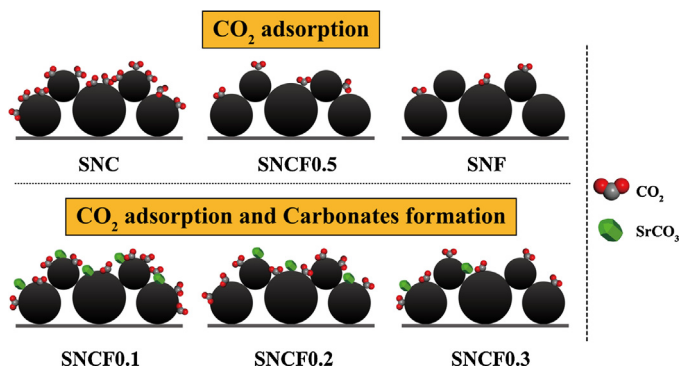
Fig. 4. Schematic diagram of two different mechanisms of interaction between CO_2 and $SrNb_{0.1}Co_{0.9-x}Fe_xO_{3-\delta}$ powders in CO_2-containing atmosphere.

Oxygen vacancies may also increase the basicity [26,34,35]. For example, Sr surface segregation on $La_{1-x}Sr_xCo_{1-y}Fe_yO_{3-\delta}$ (LSCF) could be promoted by an increase in oxygen vacancies and thus, favoring the formation of $SrCO_3$ on the surface [35]. To this end, we obtained the room temperature oxygen non-stoichiometry (δ) of $SrNb_{0.1}Co_{0.9-x}Fe_xO_{3-\delta}$ powders using iodometric titration (Fig. 5). SNCF0.1, SNCF0.2 and SNCF0.3 have relatively high oxygen non-stoichiometry scattered around 0.32 while the other compositions, SNC, SNCF0.5 and SNC have lower non-stoichiometry scattered around 0.2. Indeed, this trend strongly supported major role of oxygen vacancies toward carbonate formation.

So far, we have noted that better CO_2 resistance correlate qualitatively with increasing Fe content. It is desirable however to obtain a simple quantitative predictor, a parameter which can be utilized quite accurately to determine this property. Average metal-oxygen bond energy (ABE) represents such parameter that has been largely adopted to determine the oxygen ionic diffusion in non-stoichiometric perovskites. The energy value can be calculated from the enthalpy of formation of metal oxides, the sublimation energy of metal and the oxygen dissociation of the original oxides [36–38]. Moreover, ABE can be also used as a predictor to estimate the extent of A-site deficiency in perovskites [39]. The results of our calculations for ABE of $SrNb_{0.1}Co_{0.9-x}Fe_xO_{3-\delta}$ perovskites are plotted in Fig. 6. Despite some omitted compositions and the negative sign, the ABE becomes higher in linear proportion with increasing Fe content, which is in good agreement with the trend for ASR value deterioration (Fig. 1b). Such simple parameter however cannot predict the interaction we derived earlier using spectroscopy techniques.
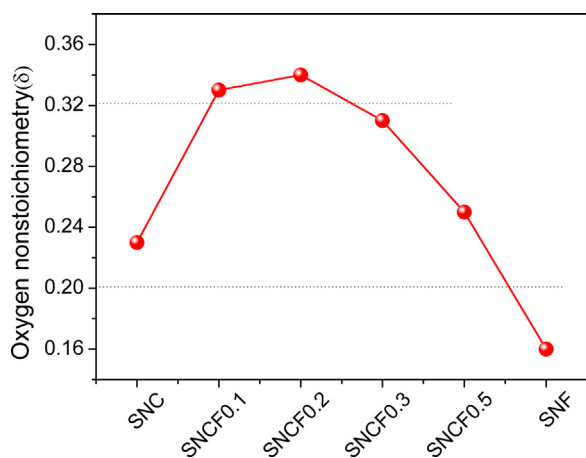

Fig. 5. The oxygen non-stoichiometries (δ) of $SrNb_{0.1}Co_{0.9-x}Fe_xO_{3-\delta}$ powders at room temperature.
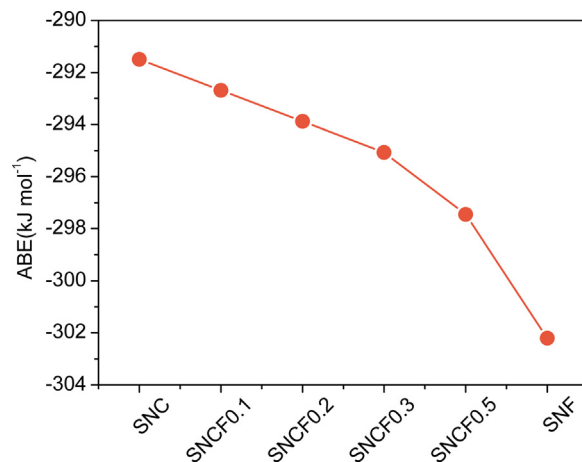

Fig. 6. Average metal-oxygen bond energy for $SrNb_{0.1}Co_{0.9-x}Fe_xO_{3-\delta}$.

4. Conclusions

CO_2 resistance of $SrNb_{0.1}Co_{0.9-x}Fe_xO_{3-\delta}$ cathode ($0 \leq x \leq 0.9$) was tested at $600\,°C$ by measuring its area specific resistance before and after the exposure with CO_2. CO_2 resistance simply increases with higher Fe content given higher energy for Fe—O bond relative to Co—O bond. This trend can be explained by the average metal-oxygen bond energy. Powder X-ray diffraction data complemented by Fourier transform-infra red spectra and CO_2-temperature programmed desorption profiles indicated substantial carbonate phase ($SrCO_3$) formation for SNCF0.1, SNCF0.2 and SNCF0.3 while is negligible for SNC, SNCF0.5 and SNF. This distinct behavior was found to correlate with the oxygen non-stoichiometry, highlighting oxygen vacancies role in promoting the carbonate formation.

Appendix A. Supplementary data

Supplementary data associated with this article can be found, in the online version, at http://dx.doi.org/10.1016/j.apcatb.2015.02.010.

References

[1] E.D. Wachsman, K.T. Lee, Science 334 (2011) 935.
[2] Z.P. Shao, S.M. Haile, Nature 431 (2004) 170.
[3] W. Zhou, Z.P. Shao, R. Ran, W.Q. Jin, N.P. Xu, Chem. Commun. (2008) 5791.
[4] W. Zhou, Z.P. Shao, R. Ran, R. Cai, Electrochem. Commun. 10 (2008) 1647.
[5] Y.L. Zhu, Z.G. Chen, W. Zhou, S.S. Jiang, J. Zhou, Z.P. Shao, ChemSusChem 6 (2013) 2294.
[6] W. Zhou, J. Sunarso, M.W. Zhao, F.L. Liang, T. Klande, A. Feldhoff, Angew. Chem. Int. Ed. 52 (2013) 14036.
[7] W. Chen, C.-S. Chen, L. Winnubst, Solid State Ionics 196 (2011) 30.
[8] K. Efimov, T. Klande, N. Juditzki, A. Feldhoff, J. Membr. Sci. 389 (2012) 205.
[9] E. Bucher, A. Egger, G.B. Caraman, W. Sitte, J. Electrochem. Soc. 155 (2008) B1218.
[10] J.X. Yi, T.E. Weirich, M. Schroeder, J. Membr. Sci. 437 (2013) 49.
[11] J.X. Yi, S.J. Feng, Y.B. Zuo, W. Liu, C.S. Chen, Chem. Mater. 17 (2005) 5856.
[12] Z. Zhao, L. Liu, X.M. Zhang, W.M. Wu, B.F. Tu, D.A. Cui, D.R. Ou, M.J. Chen, Int. J. Hydrogen Energy 38 (2013) 15361.

[13] T. Hibino, A. Hashimoto, T. Inoue, J. Tokuno, S. Yoshida, M. Sano, Science 288 (2000) 2031.
[14] M. Yano, A. Tomita, M. Sano, T. Hibino, Solid State Ionics 177 (2007) 3351.
[15] Y. Hao, Solid State Ionics 177 (2006) 2013.
[16] Z.P. Shao, C.M. Zhang, W. Wang, C. Su, W. Zhou, Z.H. Zhu, H.J. Park, C. Kwak, Angew. Chem. Int. Ed. 123 (2011) 1832.
[17] M. Nagao, M. Yano, K. Okamoto, A. Tomita, Y. Uchiyama, N. Uchiyama, T. Hibino, Fuel Cells 8 (2008) 322.
[18] Y. Wei, O. Ravkina, T. Klande, H. Wang, A. Feldhoff, J. Membr. Sci. 429 (2013) 147.
[19] A.Y. Yan, M. Yang, Z.F. Hou, Y.L. Dong, M.J. Chen, J. Power Sources 185 (2008) 76.
[20] A.Y. Yan, B. Liu, Y.L. Dong, Z.J. Tian, D.Z. Wang, M.J. Chen, Appl. Catal. B 80 (2008) 24.
[21] Z. Yáng, A.S. Harvey, L.J. Gauckler, Scr. Mater. 61 (2009) 1083.
[22] W. Chen, C.-s Chen, H.J.M. Bouwmeester, A. Nijmeijer, L. Winnubst, J. Membr. Sci. 463 (2014) 166.
[23] Y.L. Zhu, J. Sunarso, W. Zhou, S.S. Jiang, Z.P. Shao, J. Mater. Chem. A 2 (2014) 15454.
[24] R.J.H. Voorhoeve, J.P. Remeika, L.E. Trimbe, N.Y. Ann, Acad. Sci. 272 (1976) 3.
[25] O. Kubaschewski, C.B. Alcock, Metallurgical Thermochemistry, Pergamon Press Ltd., Oxford, 1979, pp. 391.
[26] W. Zhou, F.L. Liang, Z.P. Shao, Z.H. Zhu, Sci. Rep. 2 (2012) 327.
[27] B.X. Hu, M.K. Mahapatra, M. Keane, H. Zhang, P. Singh, J. Power Sources 268 (2014) 404.
[28] A.Y. Yan, V. Maragou, A. Arico, M.J. Cheng, P. Tsiakaras, Appl. Catal. B 76 (2007) 320.
[29] Z. Zhao, L. Liu, X.M. Zhang, W.M. Wu, B.F. Tu, D.R. Ou, M.J. Cheng, J. Power Sources 222 (2013) 542.
[30] J.X. Yi, M. Schroeder, T. Weirich, J. Mayer, Chem. Mater. 22 (2010) 6246.
[31] W. Zhou, Z.P. Shao, R. Ran, H.X. Gu, W.Q. Jin, N.P. Xu, J. Am. Ceram. Soc. 91 (2008) 1155.
[32] V.C. Corberan, L.G. Tejuca, A.T. Bell, J. Mater. Sci. 24 (1989) 4437.
[33] K. Nomura, Y. Ujihira, T. Haykawa, K. Takehira, Appl. Catal. A 137 (1996) 25.
[34] J. Maier, Chem. -Eur. J. 7 (2001) 4762.
[35] H.P. Ding, A.V. Virkar, M.L. Liu, F. Liu, Phys. Chem. Chem. Phys. 15 (2013) 489.
[36] J.X. Yi, J. Brendt, M. Schroeder, M. Martin, J. Membr. Sci. 387–388 (2012) 17.
[37] Y.J. Niu, W. Zhou, J. Sunarso, L. Ge, Z.H. Zhu, Z.P. Shao, J. Mater. Chem. 20 (2010) 9619.
[38] A.F. Sammells, R.L. Cook, J.H. White, J.J. Osborne, R.C. Macduff, Solid State Ionics 52 (1992) 111.
[39] E.Y. Konysheva, X.X. Xu, J.T.S. Irvine, Adv. Mater. 24 (2012) 528.